Title

Temperature and concentration dependence of the ionic transport properties of poly(ethylene oxide) electrolytes

Authors

Hoffman, Zach J
Shah, Deep B
Balsara, Nitash P

Publication Date

2021-11-01

DOI

10.1016/j.ssi.2021.115751

Solid State Ionics 370 (2021) 115751

Contents lists available at ScienceDirect

Solid State Ionics

journal homepage: www.elsevier.com/locate/ssi

Temperature and concentration dependence of the ionic transport properties of poly(ethylene oxide) electrolytes

Zach J. Hoffman [a,b,c], Deep B. Shah [a,b,c], Nitash P. Balsara [a,b,c,*]

[a] Department of Chemical and Biomolecular Engineering, University of California, Berkeley, CA 94720, USA
[b] Materials Sciences Division, Lawrence Berkeley National Laboratory, Berkeley, CA 94720, USA
[c] Joint Center for Energy Storage Research (JCESR), Lawrence Berkeley National Laboratory, Berkeley, CA 94720, USA

ARTICLE INFO

Keywords:
Polymer electrolyte
Temperature dependence
Lithium ion batteries
Concentration polarization
Concentrated solution theory
Ionic transport properties
Poly(ethylene oxide)

ABSTRACT

Even though batteries operate at different temperatures depending on their use and state of charge, little work has been done to understand the effects of temperature on the ionic transport properties of the electrolyte. The temperature dependence of these properties is important for predicting how the performance of the battery will change as a function of temperature, along with gaining fundamental insights into the underpinnings of ion transport in these electrolytes. In this study we provide the first investigation of the effect of temperature on ionic conductivity, salt diffusion coefficient, transference number, and the thermodynamic factor of a model polymer electrolyte: lithium bis(trifluoromethanesulfonyl)imide (LiTFSI) salt dissolved in poly(ethylene oxide) (PEO). These properties were measured at 70, 90, and 110 °C. As expected, we see monotonic increases in conductivity and diffusion with increasing temperature. Additionally, monotonic dependencies on temperature were obtained for the transference number and the thermodynamic factor. One presumes that concentration polarization decreases with increasing temperature due to more rapid ion transport. We use concentrated solution theory to predict concentration polarization in lithium-PEO/LiTFSI-lithium symmetric cells and thereby quantify the effect of temperature on concentration polarization.

1. Introduction

Conventional lithium ion batteries use liquid electrolytes which are mixtures of organic solvents, mainly cyclic and linear carbonates, and a lithium salt. There is considerable interest in replacing organic solvents with a polymer to address issues related to energy density and safety [1]. Polymer electrolytes are stable against lithium metal; replacing the graphite in lithium ion batteries with lithium metal results in an increase in theoretical energy density [2,3]. Polymer electrolytes are also less flammable than organic solvents, improving safety [4].

Ion transport in electrolytes is inherently complex due to the presence of two strongly interacting charged species. The thermodynamic factor and three transport parameters, conductivity, salt diffusion coefficient, and the transference number, govern ionic transport in these systems. In spite of the commercial importance of carbonate-based electrolytes and the fact that they have been studied since 1958 [5], there are few studies on the temperature dependence of the properties that govern ion transport [6–8]. Such studies are important for two reasons. First, batteries are operated at different temperatures based on ambient conditions and state of health of the battery [9]. Second, temperature dependent measurements provide fundamental insight that cannot be gleaned from measurements at a fixed temperature.

Mixtures of poly(ethylene oxide) (PEO) and bis(trifluoromethanesulfonyl)imide lithium salt (LiTFSI) are commonly used polymer electrolytes. While there are numerous reports of the dependence of ionic conductivity on temperature [10–13], there is little work on the temperature dependence of the other relevant properties [14,15]. The objective of this paper is to present measurements of all the properties that affect ion transport in PEO/LiTFSI mixtures as a function of temperature.

2. Experimental

2.1. Electrolyte preparation

Electrolytes for most of the measurements reported in this paper were prepared by adding LiTFSI salt (Sigma Aldrich) to 10 kg/mol PEO with a dispersity of 1.03 (Sigma Aldrich), then dissolving in

* Corresponding author at: Department of Chemical and Biomolecular Engineering, University of California, Berkeley, CA 94720, USA.
E-mail address: nbalsara@berkeley.edu (N.P. Balsara).

https://doi.org/10.1016/j.ssi.2021.115751
Received 21 July 2021; Received in revised form 27 August 2021; Accepted 29 August 2021
Available online 13 September 2021

tetrahydrofuran (THF). The mixtures were stirred at 60 °C until completely dissolved, dried on a hotplate for at least 12 h to evaporate the THF, and then dried at 90 °C under vacuum to remove any residual solvent. These procedures were previously reported by our group [11,16]. Electrolytes were produced with salt concentrations of r values from 0.02 to 0.3, where r is the ratio of lithium ions to ethylene oxide moieties ($r = [Li^+]/[EO]$). The density of our electrolytes, ρ, was assumed to follow that previously measured in our group for PEO samples of 5 and 35 kg/mol [11,17], and was used to calculate the molar salt concentration, c, using the equation

$$c = \frac{\rho r}{M_{EO} + rM_{salt}}, \tag{1}$$

with M_{EO} and M_{salt} being 44.05 g/mol and 287.09 g/mol, respectively. In our calculations we also use m, the molality of the electrolyte, which is calculated using

$$m = \frac{r}{M_{EO}}. \tag{2}$$

Values for c, ρ, and m for the range of salt concentrations of interest can be found in ref. [11].

We found that concentration cells made with 10 kg/mol PEO at 110 °C gave irreproducible results, presumably due to the liquid like nature of this polymer at 110 °C. We therefore made electrolytes using the same process described above but with 275 kg/mol PEO for constructing these cells. Gao and Balsara have shown that electrochemical properties show no discernable dependence on molecular weight [18].

2.2. Electrochemical characterization

Preparation of electrochemical cells was done in an argon-filled VAC glovebox with water and oxygen levels below 1 ppm.

Conductivity cells were constructed by filling a silicone spacer (McMaster-Carr) with a thickness of 508 μm and inner diameter of 3.175 mm with the electrolyte and pressing a 200 μm stainless-steel shim (MTI Corporation) blocking electrode on each side of the spacer. Nickel current collectors (MTI Corporation) were attached to the cell using Kapton tape. The cells were then vacuum sealed inside aluminum laminated pouch material (MTI Corporation) before being removed from the glovebox.

The conductivity cells were annealed for 2 h at 90 °C.The temperature was controlled with a custom built heating stage. Using a Biologic VMP3 potentiostat, ac impedance spectroscopy was performed with an amplitude of 60 mV, and a frequency range of 1 MHz to 1 Hz. After these measurements were made, the cells were brought back into the glove box for deconstruction and the final thickness of the electrolyte was measured.

The ionic conductivity (κ) was calculated using Eq. (3)

$$\kappa = \frac{L}{R_b A_E} \tag{3}$$

where L is the thickness of the separator, A_E is the electrochemically active area of the electrolyte, and R_b is the bulk resistance of the electrolyte, which is found by fitting the conductivity data to an equivalent circuit.

Lithium symmetric cells were used to perform both current fraction and restricted diffusion experiments. 508 μm thick silicone spacer material with an inner diameter of 3.175 mm was filled with electrolyte, and lithium foil (MTI corporation) of measured thicknesses ranging from 180 to 350 μm was pressed on each side of the spacer material, followed by 200 μm thick stainless steel shims. Nickel current collectors were adhered to the stack using Kapton tape. The stacks were sealed in laminated aluminum pouch material, and then removed from the glovebox.

The lithium symmetric cells were first annealed for 3 h at 90 °C and then conditioned with 4 cycles of ±0.02 mA/cm^2, each for 5 h. This conditioning was performed to ensure the formation of a stable interfacial region indicated by consistent values of a cell's interfacial resistance and its potential response to each cycle. The cells were then subjected to a constant +10 mV for 20 min followed by an impedance measurement and then this was repeated to observe the changes in resistances as the system reached a steady state current. This process was replicated for −10 mV, +20 mV, and −20 mV. The current fraction (ρ_+) is calculated by comparing the steady state current (i_{ss}) and the initial current density (i_0). In ideal electrolytes this relation can be simply written as

$$\rho_+ = \frac{i_{ss}}{i_0}. \tag{4}$$

In polymer electrolytes it is necessary to account for the potential drop cause by the electrode/electrolyte interface which results in

$$\rho_+ = \frac{i_{ss}\left(\Delta V - i_0 R_{i,0}\right)}{i_0\left(\Delta V - i_{ss} R_{i,ss}\right)}, \tag{5}$$

as developed by Bruce and Vincent [19], where ΔV is the applied potential, and $R_{i,0}$ and $R_{i,ss}$ are the initial and steady state interfacial impedances measured using impedance spectroscopy, respectively. Practically, it is challenging to measure i_0 accurately without sufficiently fast sampling rates. Instead, we use a calculated initial current i_Ω which can be determined from easily measured parameters using

$$i_\Omega = \frac{\Delta V}{R_{b,0} + R_{i,0}}, \tag{6}$$

where $R_{b,0}$ is the initial resistance of the bulk. Combining Eqs. (5) and (6) gives

$$\rho_+ = \frac{i_{ss}\left(\Delta V - i_0 R_{i,0}\right)}{i_\Omega\left(\Delta V - i_{ss} R_{i,ss}\right)}. \tag{7}$$

At the end of the current fraction experiments restricted diffusion experiments are performed, where the cells were allowed to relax for 3 h [20]. This relaxation of the potential in the cell can be fit to

$$U(t) = k_0 + ae^{-bt}, \tag{8}$$

where k_0 is the fitted offset voltage, and a and b are fit parameters. Using b, the salt diffusion coefficient can be found using the formula

$$D = \frac{L^2 b}{\pi^2}. \tag{9}$$

These fits are performed while increasing the lower bounds of time so that the nondimensional number α, according to

$$\alpha = \frac{Dt}{L^2}, \tag{10}$$

reaches a value above 0.05, as established by Thompson and Newman [21]. Concentration cells were used to measure the open circuit potential produced from the concentration gradient between two electrolytes with different amounts of LiTFSI. The cell design was based on procedures outlined in ref. [11]. 508 μm thick silicone spacer material was cut into rectangular shapes with an internal channel of about 2.5 cm by 3 mm. The silicone channels were placed on a similarly sized rectangle of nickel foil to act as a base. Electrolyte was then placed into each half of the channel, with one half always containing the reference electrolyte ($r = 0.06$, $\ln m = 0.31$). Lithium foil was placed on the ends of the channel, and nickel current collectors were attached to the lithium foil. A rectangle of silicone spacer material was then placed on top of the cell to maintain the construction of the cell during sealing and to help ensure there was enough pressure within the cell to prevent leakage of the electrolyte. The cells were then sealed inside laminated aluminum pouch material and brought to the temperature of interest using a

heating stage. The voltage was measured until it reached a plateau, at which point the average potential was measured and recorded as the open circuit potential of that salt concentration (U).

For conductivity cells, and lithium symmetric cells, the average value of at least three measurements is reported with the standard deviation as the error bar. The error for the transference number was calculated using the equation

$$\left(\delta t_+^0\right)^2 = \left(\frac{dt_+^0}{d\rho_+}\right)^2 \delta{\rho_+}^2 + \left(\frac{dt_+^0}{d\kappa}\right)^2 \delta\kappa^2 + \left(\frac{dt_+^0}{dD}\right)^2 \delta D^2 + \left(\frac{dt_+^0}{d\left[dU/dlnm\right]}\right)^2 \delta\left[dU/dlnm\right]^2. \quad (11)$$

Where δt_+^0 indicates the error of the transference number, and $\delta\rho_+$, $\delta\kappa$, δD, and $\delta[dU/dlnm]$ are the values of error for each parameter. The same general equation was used to calculate the error of the thermodynamic factor.

3. Results and discussion

Fig. 1a shows the ionic conductivity of PEO/LiTFSI electrolytes as a function of temperature for the seven different electrolytes. The ionic conductivity, κ, increases monotonically with temperature as expected, but this increase depends on salt concentration. It is customary to use the Vogel-Tamman-Fulcher equation to describe the temperature dependence of conductivity:

$$\kappa(T) = A\left[exp\left(-\frac{E_a}{R(T - T_g + 50)}\right)\right], \quad (12)$$

where A and E_a are parameters found by fitting the experimental data, R is the universal gas constant, and T_g is the glass transition temperature of the electrolyte. The glass transition temperature of PEO/LiTFSI electrolytes was taken from the work of Perrier et al. [22], and Pesko et al. [12] The lines in Fig. 1b represent these fits, and the dependence of T_g, A, and E_a are given in Table S1. VTF analysis assumes that ion transport is governed by segmental relaxation and the VTF parameters quantify this relaxation. In Fig. 1b we plot κ as a function of $1000/(T\text{-}T_g + 50)$ on a semi-log plot. These plots are linear, which is consistent with the literature [12,13]. While the slopes obtained at different salt concentrations are similar, the intercepts are not. This implies that T_g is not the only parameter that affects conductivity. For a given value of $1000/(T\text{-}T_g + 50)$ the maximum conductivity is obtained at a salt concentration of $r = 0.12$.

An alternative approach for examining electrolyte conductivity was proposed by Mongcopa et al. [23]

$$\kappa(r) = K(T)r\left[exp\left(-\frac{r}{r_{max}(T)}\right)\right], \quad (13)$$

where $K(T)$ is a temperature dependent constant that is related to the extent of salt dissociation, and the term within the square brackets represents frictional interactions between the salt ions and the polymer. Eq. (13) has two temperature dependent fitting parameters. It can readily be seen that the parameter relating to the frictional interactions, $r_{max}(T)$, coincides with the salt concentration at which the conductivity is maximized.

In Fig. 2a, we plot conductivity as a function of r at different temperatures. The curves in Fig. 2a are fits of Eq. (13) with $K(T)$ and $r_{max}(T)$ as fitting parameters. Both parameters are linear functions of T:

$$K(T) = 9.904 \times 10^{-4}\ \mathrm{T} - 3.95 \times 10^{-2}\ (\mathrm{S/cm}) \quad (14)$$

$$r_{max}(T) = 6.69 \times 10^{-4}\ \mathrm{T} + 1.30 \times 10^{-2} \quad (15)$$

An important parameter is the value of the maximum conductivity obtained at each temperature, κ_{max}. We use fits of Eq. (13) to determine κ_{max} and these results are shown in Fig. 2c. κ_{max} increases by about a factor of 3 when temperature is increased from 70 to 110 °C.

Fig. 3a shows the mutual salt diffusion coefficient (D) measured using restricted diffusion experiments, as a function of r and T. In general, we see that D decreases as r increases. The trend is approximately linear at all temperatures; Fig. 3a shows linear fits through the data.

The slopes and intercepts respectively of the data are: -1.6575×10^{-7} cm^2/s and 6.979×10^{-8} cm^2/s at 70 °C, -2.816×10^{-7} cm^2/s and 1.133×10^{-7} cm^2/s at 90 °C, and -3.205×10^{-7} cm^2/s and 1.679×10^{-7} cm^2/s at 110 °C.

At a given salt concentration, the diffusion coefficient increases by about a factor of 3 when temperature is increased from 70 to 110 °C. In this respect, we see similarities between the temperature dependencies of conductivity (Fig. 2a) and diffusion coefficients (Fig. 3a).

Fig. 3b shows the current fraction (ρ_+) measured by the Bruce-Vincent method as a function of r and T. Unlike κ and D, ρ_+ is, to a

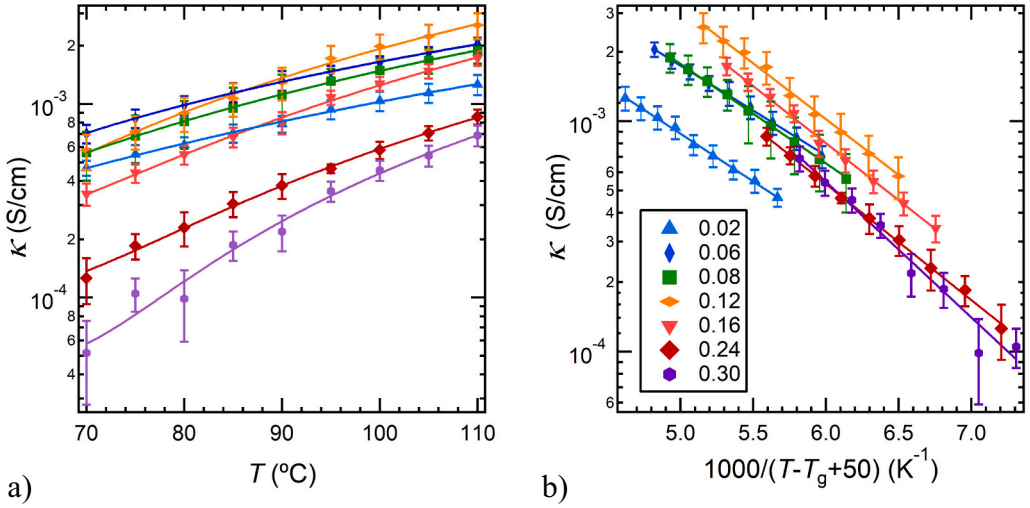

Fig. 1. (a) Conductivity of PEO/LiTFSI electrolytes as a function of temperature, T, and polynomial fits of the data. (b) Vogel-Tammann-Fulcher plot of conductivity of the electrolytes, T_g is the glass transition temperature of each electrolyte, and it depends on salt concentration. Salt concentration, r, for each data set is given in the legend.

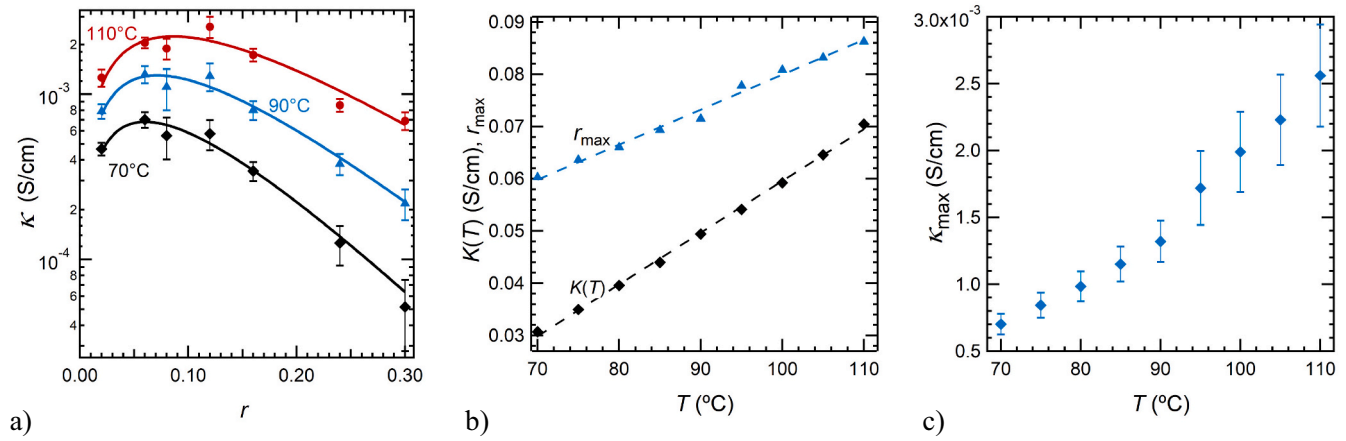

Fig. 2. (a) Conductivity of PEO/LiTFSI electrolytes as a function of salt concentration, r, at 70, 90, and 110 °C. (b) The fit parameters $K(T)$, and r_{max} from Eq. (13) plotted as a function of temperature. r_{max} is the salt concentration at which conductivity is maximized, and K(T) is the prefactor in Eq. (13). (c) The maximum value of conductivity, κ_{max}, plotted as a function of temperature.

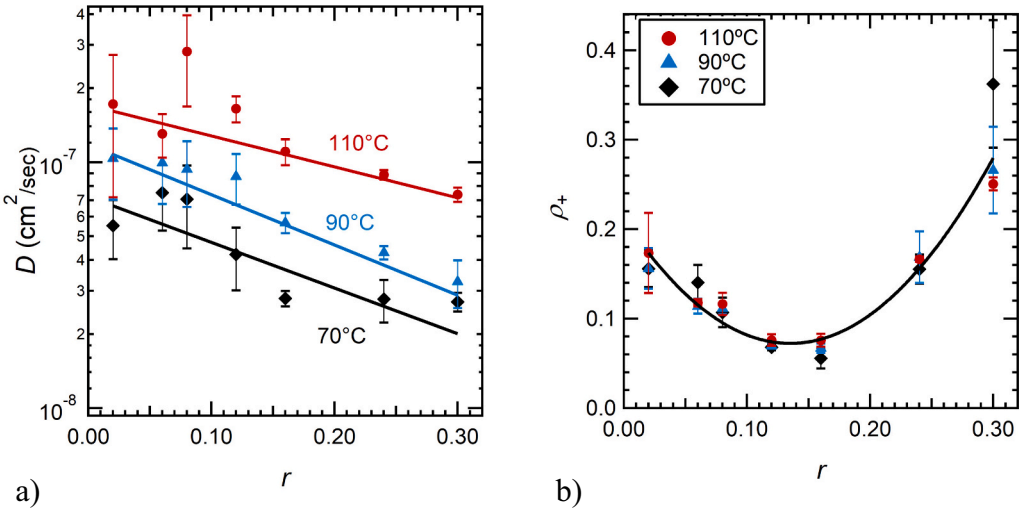

Fig. 3. (a) Salt diffusion coefficient and (b) current fraction as a function of salt concentration, r, at 70, 90, and 110 °C. Fits of the data are included as solid lines. All the current fraction data have been fit to a single curve.

reasonable approximation, independent of temperature between 70 and 110 °C. This is consistent with previous studies in the literature [14,15]. The curve in Fig. 3b, is a polynomial fit through all three data sets:

$$\rho_+(r) = 7.632r^2 - 2.063r + 0.212 \quad (16)$$

The conductivity of an electrolyte reflects the mobility of both the cation and the anion. In most batteries, only the cation participates in the reactions occurring within the electrodes. The symmetric lithium-lithium cell is the simplest construct to study the efficacy of an electrolyte in batteries. The ratio of the current density and the applied potential gradient can be regarded as an effective conductivity. In the limit of small applied potentials, this effective conductivity is equal to the product $\kappa\rho_+$ [24–27]. In Fig. 4 we plot $\kappa\rho_+$ as a function of r for three different temperatures. The general features of the dependence of $\kappa\rho_+$ on r are similar at all temperatures. In the low concentration regime, $0 < r \leq 0.16$, $\kappa\rho_+$ approaches a maximum at $r = 0.06$, irrespective of temperature. Note that this salt concentration differs substantially from the salt concentration for which κ is maximized. In this low concentration regime, the decrease in conductivity with increasing salt concentration is steepest at 70 °C; $\kappa\rho_+$ at $r = 0.16$ is a factor of 5 smaller than that at $r = 0.06$. This decrease is significantly lower at 110 °C, where $\kappa\rho_+$ at $r = 0.16$ is only a factor of 2 smaller than that at $r = 0.06$. There is an abrupt change in the dependence of $\kappa\rho_+$ on r at $r = 0.16$. In the high salt concentration regime, $0.16 \leq r \leq 0.30$, $\kappa\rho_+$ is independent of r. In other words, the decrease in κ with increasing r in this regime is compensated for by an increase in ρ_+. Computer simulations have established that in the dilute limit, lithium ions are coordinated by six oxygen atoms [28,29]. At $r = 1/6 = 0.166$, all the oxygen atoms in the system are coordinated with lithium ions. It is interesting that the division between the two regimes seen in Fig. 4 occurs at this value of r.

The final experiment required for completing the full electrochemical characterization of PEO/LiTFSI mixtures is the measurement of the open circuit potential, U, with the use of concentration cells. In these cells, a reference electrolyte with $r = 0.06$ ($\ln m = 0.31$) is brought in contact with electrolytes of varying concentrations. It is customary to present such data on a plot of U versus $\ln m$ [30]. The data obtained are shown in Fig. 5, along with previously published data [31] obtained from a PEO sample with a molecular weight of 275 kg/mol at 90 °C. All data sets are similar: the slope of U versus $\ln m$ is small when $\ln m$ is less than zero compared to when $\ln m$ is greater than zero. We use a single 4th order polynomial to fit all the data in Fig. 5a:

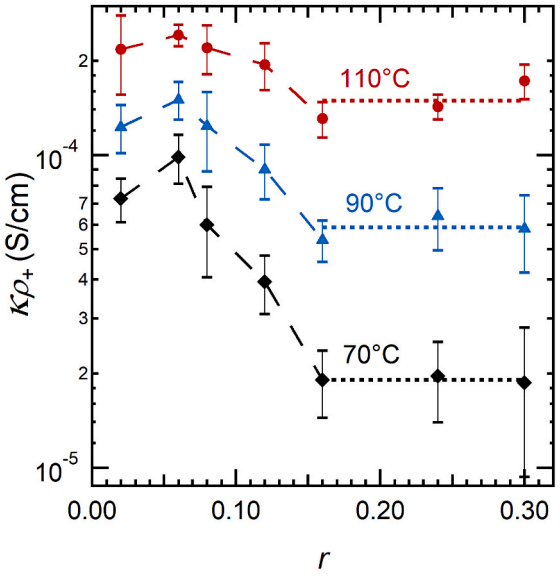

Fig. 4. The product of the current fraction and the conductivity of the electrolytes, $\kappa\rho_+$. as a function of salt concentration, r, at 70, 90, and 110 °C. This product may be regarded as the effective conductivity in the limit of small applied potentials.

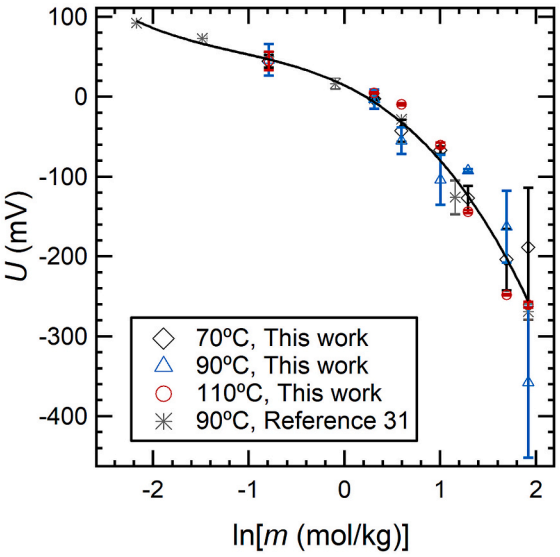

Fig. 5. Open-circuit potential across concentration cells (U) plotted as a function of the natural logarithm of the molality of salt in the electrolyte (ln$m$). In addition to data measured in this study, we have included data from ref. [31]. All data sets were fit to a single curve shown in the figure.

$$U(lnm) = -8.62(lnm)^3 - 29.95(lnm)^2 - 56.46(lnm) - 20.56 \text{ (mV)} \quad (17)$$

Conductivity of an electrolyte can be measured in both conductivity cells (blocking electrodes) and lithium symmetric cells (nonblocking electrodes). In Fig. 6 we compare these measurements for our PEO/LiTFSI mixtures. The solid and dashed curves in Fig. 6 represent fits of Eq. (13) through these data. In general, the nonblocking conductivity is slightly lower than the blocking conductivity. At $r = 0.30$ however, significantly lower nonblocking conductivities are obtained at 70 and 90 °C. We note in passing that in many systems there are much more significant differences between blocking and nonblocking conductivities [32].

The measurement of D, κ, ρ_+, and U as a function of salt concentration enables calculation of the cationic transference number with respect to the solvent, t_+^0, and the thermodynamic factor, T_f, using the following equations,

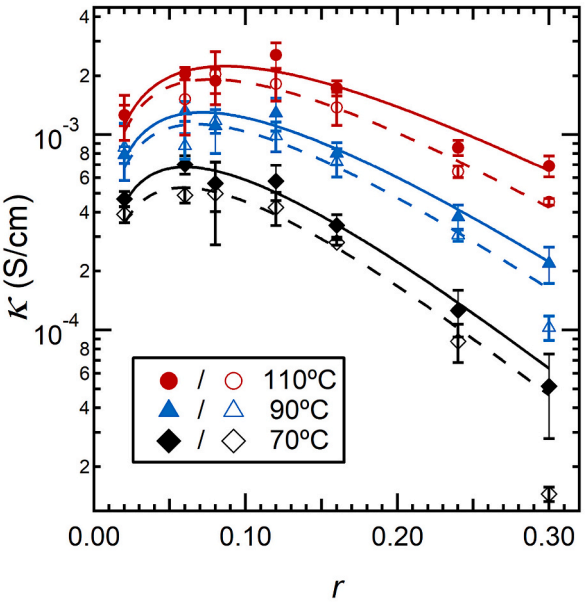

Fig. 6. Conductivity measured with blocking and nonblocking electrodes, plotted as a function of r at 70, 90, and 110 °C. The solid curves are fits of the blocking conductivity data, represented by filled points, and the dashed curves are fits of the nonblocking conductivity, represented by hollow points.

$$t_+^0 = 1 + \left(\frac{1}{\rho_+} - 1\right)\frac{FDc}{\kappa}\left(\frac{dlnm}{dU}\right), \quad (18)$$

and

$$T_f = 1 + \frac{dln\gamma_\pm}{dlnm} = \frac{\kappa}{\nu RTDc\left(\frac{1}{\rho_+} - 1\right)}\left(\frac{dU}{dlnm}\right)^2. \quad (19)$$

In these equations, c is the concentration of lithium ions in the electrolyte (moles/L), and $\frac{dU}{dlnm}$ is the derivative of the curve of U vs ln$m$. We use Eqs. (13)–(17) along with the linear equations describing the diffusion coefficient noted previously to calculate the transference number and thermodynamic factor at different salt concentrations, and the results are shown in Fig. 7. The dependence of t_+^0 on r is similar at all temperatures with the minimum at $r = 0.16$, the salt concentration at which all of the oxygens in the PEO chains are coordinated with lithium. The transference number at this concentration is negative, implying the presence of negatively charged clusters, consistent with previous studies on PEO/LiTFSI [11,31]. The transference number at a given salt concentration increases when the temperature is changed from 70 to 90 °C. The same is true when changing the temperature from 90 to 110 °C, but the increase is much smaller. There are relatively few systems where the rigorously defined t_+^0 is defined explicitly. In conventional lithium-ion battery electrolytes comprising mixtures of ethylene carbonate, dimethyl carbonate, and $LiPF_6$, Landesfeind and Gasteiger [8] report that t_+^0 increases with increasing temperature, while Reimers et al. [6] infer that t_+^0 is independent of temperature in mixtures of ethylene carbonate, dimethyl carbonate, and polycarbonate. T_f shows a similar temperature dependence as t_+^0, where at a given salt concentration T_f will increase as temperature is changed from 70 to 90 °C, and increase less from 90 to 110 °C.

The full characterization of an electrolyte provides information that can be used to model the salt concentration profiles inside a lithium-lithium symmetric cell as a function of applied current density, i,

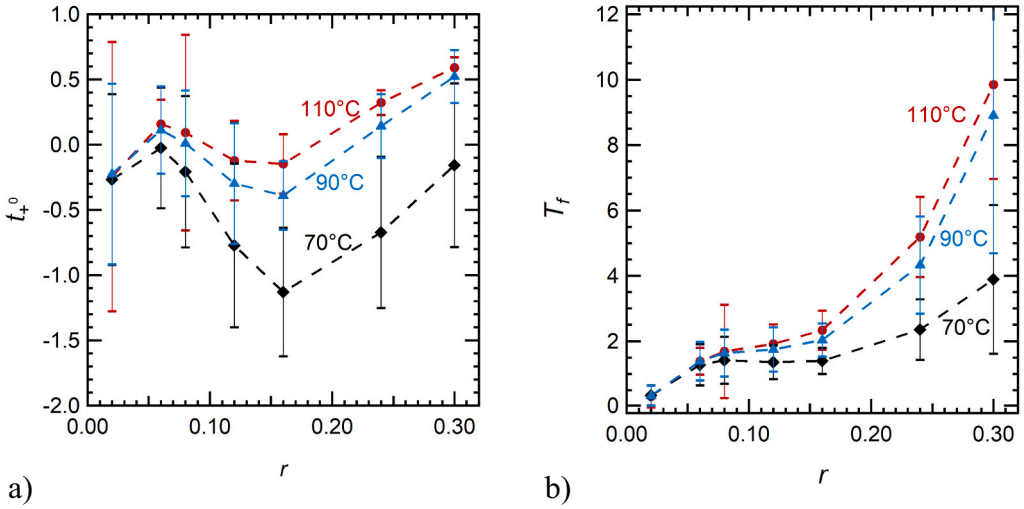

Fig. 7. (a) Cationic transference number with respect to the solvent velocity and (b) thermodynamic factor plotted as a function of salt concentration, r at 70, 90, and 110 °C.

using concentrated solution theory [27]. We define x as the distance from the positive electrode and assume that the negative electrode is located at $x = L$, where L is the thickness of the lithium-lithium symmetric cell. The dependence of r on x is given in ref. [33],

$$\int_{r(x=0)}^{r(x)} \frac{D(r)c(r)}{r\left(1-t_+^0(r)\right)}dr = -\frac{iL}{F}\left(\frac{x}{L}\right) \tag{20}$$

The dependence of D and t_+^0 are described by Figs. 3a and 7a. This enables calculation of the integrand on the left side of Eq. (20), $\frac{Dc}{r\left(1-t_+^0\right)}$. The integrand is approximated by polynomial expression,

$$\frac{D(r)c(r)}{r\left(1-t_+^0(r)\right)} = ar^4 + br^3 + cr^2 + dr + e, \tag{21}$$

and the constants a through e are obtained by a least squares fit through the experimental data. The values of these parameters at each temperature are given in Table S4.

We present results for a constant current density of 0.2 mA/cm^2, and for average salt concentrations, r_{av}, of 0.065 and 0.10. Eq. (20) is solved iteratively to obtain $r(x)$ such that the calculated r_{av} agrees with the targeted value. The results for $r_{av} = 0.065$ are shown in Fig. 8a. Considerable concentration polarization is seen at 70 °C: $r(x/L = 0) = 0.13$, while $r(x/L = 1) = 0.02$. Increasing the temperature to 90 °C reduces the magnitude of concentration polarization, and increasing the temperature to 110 °C reduces the magnitude of concentration polarization further. The qualitative trend is not surprising as the rate of ion transport is often improved by increasing temperature. The results for r_{av} of 0.10 are shown in Fig. 8b. Larger concentration gradients are seen in this case when compared to $r_{av} = 0.065$ at all temperatures. Increasing the temperature to 110 °C reduces concentration polarization by a factor of about 3 at $r = 0.065$ and a factor of 5 at $r = 0.10$. This is surprising because the conductivity at $r_{av} = 0.10$ is higher than that at $r_{av} = 0.065$, pointing to the importance of complete electrochemical characterization.

4. Conclusions

In this study we have performed the first investigation of the temperature effects on full electrochemical characterization of a standard

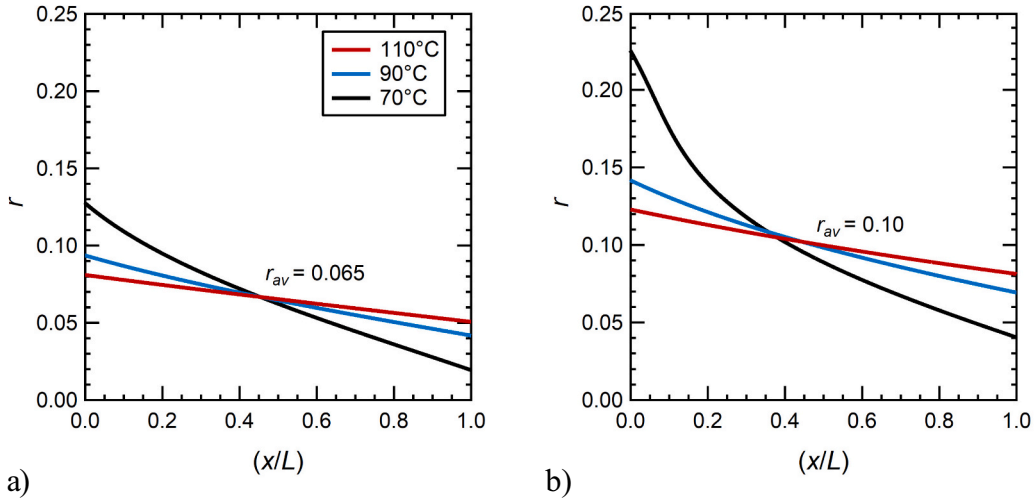

Fig. 8. LiTFSI concentration profiles modeled using concentrated solution theory at 70, 90, and 110 °C in lithium-PEO/LiTFSI-lithium cells with average salt concentrations of (a) $r_{av} = 0.065$ (b) $r_{av} = 0.10$ at a fixed current density of 0.2 mA/cm^2. $x/L = 0$ corresponds to the anode and $x/L = 1$ corresponds to the cathode, where L is the electrolyte thickness of 500 μm.

polymer electrolyte: PEO/LiTFSI. The electrochemical properties, which included κ, D, t_+^0, and T_f, of these electrolytes were measured at 70, 90, and 110 °C. κ and D increase monotonically with temperature. t_+^0 shows a minimum at $r = 0.16$ for all temperatures and has a monotonic dependence on temperature and a non-monotonic dependence on concentration. T_f increases with increasing salt concentration at all temperatures. We used the measured transport parameters to predict concentration polarization in symmetric lithium-lithium cells at different temperatures. We find that concentration polarization decreases by factors between 3 and 5 in our temperature window, depending on salt concentration.

Symbols

PEO	poly(ethylene oxide)
LiTFSI	lithium bis(trifluoromethanesulfonyl)imide
D	salt diffusion coefficient (cm^2/s)
κ	ionic conductivity (S/cm)
ρ_+	current fraction
T_f	thermodynamic factor
t_+^0	fully defined transference number
r	molar ratio of lithium ions to ethylene oxide
L	electrolyte thickness (cm.)
A_E	electrolyte area (cm^2)
$R_{b,0}$	initial bulk resistance of electrolyte (Ω)
$R_{b,ss}$	steady state bulk resistance of electrolyte (Ω)
i_{ss}	steady state current (mA)
i_Ω	calculated initial current (mA)
ΔV	potential drop (mV)
$R_{i,0}$	initial interfacial resistance (Ω)
$R_{i,ss}$	steady state interfacial resistance (Ω)
U	open-circuit potential (mV)
a,b	fit parameters for Eq. (8)
k_0	offset voltage (mV)
α	non-dimensional time for diffusion
t	time (s)
i_o	initial current (mA)
T	temperature (°C)
ν	number of ions produced from salt dissociation
ν_+	number of cations produced from salt dissociation
z_+	charge of cations
$\gamma_\pm$	mean molal activity coefficient
$dU/d\ln m$	derivative of the curve of U plotted vs lnm
m	molality (mol/kg)
c	salt concentration (M)
ρ	density (g/L)
A	VTF prefactor (S/cm)
E_a	effective activation energy (kJ/mol)
R	universal gas constant (kJ/mol K)
T_g	glass transition temperature (°C)
$K(T)$	conductivity prefactor (S/cm)
$r_{max}(T)$	conductivity fit parameter
T_f	thermodynamic factor
r_{av}	average salt concentration

Declaration of Competing Interest

The authors declare no competing financial interests.

Acknowledgements

This work was intellectually led by the Joint Center for Energy Storage Research (JCESR), an Energy Innovation Hub funded by the U.S. Department of Energy, Office of Science, Office of Basic Energy Science, under Contract No. **DE-AC02-06CH11357**, which supported characterization work conducted by Z.J.H. and D.B.S. under the supervision of N.P.B. The authors thank Louise Frenck and Kevin Gao for useful discussion related to this work.

Appendix A. Supplementary data

Supplementary data to this article can be found online at https://doi.org/10.1016/j.ssi.2021.115751.

References

[1] K. Xu, Nonaqueous liquid electrolytes for lithium-based rechargeable batteries, Chem. Rev. 104 (10) (Oct. 2004) 4303–4417, https://doi.org/10.1021/CR030203G.
[2] M.M. Thackeray, C. Wolverton, E.D. Isaacs, Electrical energy storage for transportation—approaching the limits of, and going beyond, lithium-ion batteries, Energy Environ. Sci. 5 (7) (Jun. 2012) 7854–7863, https://doi.org/10.1039/C2EE21892E.
[3] S. Choudhury, et al., Solid-state polymer electrolytes for high-performance lithium metal batteries, Nat. Commun. 2019 101 10 (1) (Sep. 2019) 1–8, https://doi.org/10.1038/s41467-019-12423-y.
[4] D.H.C. Wong, et al., Nonflammable perfluoropolyether-based electrolytes for lithium batteries, Proc. Natl. Acad. Sci. 111 (9) (Mar. 2014) 3327–3331, https://doi.org/10.1073/PNAS.1314615111.
[5] W.S. Harris, Electrochemical Studies in Cyclic Esters, 1958.
[6] L.O. Valoen, J.N. Reimers, Transport properties of LiPF[sub 6]-based Li-ion battery electrolytes, J. Electrochem. Soc. (2005), https://doi.org/10.1149/1.1872737.
[7] H. Lundgren, M. Behm, G. Lindbergh, Electrochemical characterization and temperature dependency of mass-transport properties of LiPF 6 in EC:DEC, J. Electrochem. Soc. (2015), https://doi.org/10.1149/2.0641503jes.
[8] J. Landesfeind, H.A. Gasteiger, Temperature and concentration dependence of the ionic transport properties of lithium-ion battery electrolytes, J. Electrochem. Soc. (2019), https://doi.org/10.1149/2.0571912jes.
[9] M.B. Stevens, Hybrid fuel cell vehicle powertrain development considering power source degradation, Design (2008) 1–228.
[10] A.A. Teran, M.H. Tang, S.A. Mullin, N.P. Balsara, Effect of molecular weight on conductivity of polymer electrolytes, Solid State Ionics (2011), https://doi.org/10.1016/j.ssi.2011.09.021.
[11] D.M. Pesko, et al., Negative transference numbers in poly(ethylene oxide)-based electrolytes, J. Electrochem. Soc. (2017), https://doi.org/10.1149/2.0581711jes.
[12] D.M. Pesko, et al., Effect of monomer structure on ionic conductivity in a systematic set of polyester electrolytes, Solid State Ionics (2016), https://doi.org/10.1016/j.ssi.2016.02.020.
[13] D. Devaux, R. Bouchet, D. Glé, R. Denoyel, Mechanism of ion transport in PEO/LiTFSI complexes: Effect of temperature, molecular weight and end groups, Solid State Ionics (2012), https://doi.org/10.1016/j.ssi.2012.09.020.
[14] M.M. Hiller, M. Joost, H.J. Gores, S. Passerini, H.D. Wiemhöfer, The influence of interface polarization on the determination of lithium transference numbers of salt in polyethylene oxide electrolytes, Electrochim. Acta (2013), https://doi.org/10.1016/j.electacta.2013.09.138.
[15] K. Pożyczka, M. Marzantowicz, J.R. Dygas, F. Krok, Ionic conductivity and lithium transference number of poly(ethylene oxide):litfsi system, Electrochim. Acta (2017), https://doi.org/10.1016/j.electacta.2016.12.172.
[16] D.A. Gribble, et al., Comparing experimental measurements of limiting current in polymer electrolytes with theoretical predictions, J. Electrochem. Soc. (2019), https://doi.org/10.1149/2.0391914jes.
[17] W.S. Loo, K.I. Mongcopa, D.A. Gribble, A.A. Faraone, N.P. Balsara, Investigating the effect of added salt on the chain dimensions of poly(ethylene oxide) through small-angle neutron scattering, Macromolecules (2019), https://doi.org/10.1021/acs.macromol.9b01509.
[18] K.W. Gao, N.P. Balsara, Electrochemical properties of poly(ethylene oxide) electrolytes above the entanglement threshold, Solid State Ionics 364 (Jun. 2021) 115609, https://doi.org/10.1016/J.SSI.2021.115609.
[19] E. Staunton, Y.G. Andreev, P.G. Bruce, Factors Influencing the Conductivity of Crystalline Polymer Electrolytes, 2007, https://doi.org/10.1039/b601945e.
[20] J. Newman, T.W. Chapman, Restricted diffusion in binary solutions, AICHE J. (1973), https://doi.org/10.1002/aic.690190220.
[21] S.D. Thompson, J. Newman, Differential diffusion coefficients of sodium polysulfide melts, J. Electrochem. Soc. (2019), https://doi.org/10.1149/1.2096451.
[22] M. Perrier, S. Besner, C. Paquette, A. Vallée, S. Lascaud, J. Prud'homme, Mixed-alkali effect and short-range interactions in amorphous poly(ethylene oxide) electrolytes, Electrochim. Acta (1995), https://doi.org/10.1016/0013-4686(95)00151-4.
[23] K.I.S. Mongcopa, et al., Relationship between segmental dynamics measured by quasi-elastic neutron scattering and conductivity in polymer electrolytes, ACS Macro Lett. (2018), https://doi.org/10.1021/acsmacrolett.8b00159.
[24] N.P. Balsara, J. Newman, Relationship between steady-state current in symmetric cells and transference number of electrolytes comprising univalent and multivalent ions, J. Electrochem. Soc. (2015), https://doi.org/10.1149/2.0651514jes.
[25] P.G. Bruce, C.A. Vincent, Steady state current flow in solid binary electrolyte cells, J. Electroanal. Chem. (1987), https://doi.org/10.1016/0022-0728(87)80001-3.

[26] J. Doyle, Fuller Marc, Newman Thomas, The importance of the lithium ion transference number in lithium polymer cells, Electrochim. Acta1 39 (13) (1993) 2073–2081, https://doi.org/10.1016/0013-4686(94)85091-7 [Online]. Available:.
[27] J. Newman, K.E. Thomas-Alyea, Electrochemical Systems, Third edition, 2004.
[28] O. Borodin, G.D. Smith, Mechanism of ion transport in amorphous poly(ethylene oxide)/ LiTFSI from molecular dynamics simulations, Macromolecules (2006), https://doi.org/10.1021/ma052277v.
[29] D. Diddens, A. Heuer, O. Borodin, Understanding the lithium transport within a rouse-based model for a PEO/LiTFSI polymer electrolyte, Macromolecules (2010), https://doi.org/10.1021/ma901893h.
[30] Y. Ma, The measurement of a complete set of transport properties for a concentrated solid polymer electrolyte solution, J. Electrochem. Soc. (1995), https://doi.org/10.1149/1.2044206.
[31] D.M. Pesko, S. Sawhney, J. Newman, N.P. Balsara, Comparing two electrochemical approaches for measuring transference numbers in concentrated electrolytes, J. Electrochem. Soc. (2018), https://doi.org/10.1149/2.0231813jes.
[32] M.D. Galluzzo, J.A. Maslyn, D.B. Shah, N.P. Balsara, Ohm's law for ion conduction in lithium and beyond-lithium battery electrolytes, J. Chem. Phys. (2019), https://doi.org/10.1063/1.5109684.
[33] D.M. Pesko, Z. Feng, S. Sawhney, J. Newman, V. Srinivasan, N.P. Balsara, Comparing cycling characteristics of symmetric lithium-polymer-lithium cells with theoretical predictions, J. Electrochem. Soc. (2018), https://doi.org/10.1149/2.0921813jes.